

# Dynamics of Resonances in Strongly Interacting Systems

J. Knoll<sup>1</sup>, F. Riek<sup>1</sup>, Yu. B. Ivanov<sup>1,2</sup> and D.N. Voskresensky<sup>1,3</sup>

<sup>1</sup> Gesellschaft für Schwerionenforschung mbH, Planckstr. 1  
64291 Darmstadt, Germany

<sup>2</sup> Kurchatov Institute, Kurchatov sq. 1, Moscow 123182, Russia

<sup>3</sup> Moscow Institute for Physics and Engineering, Kashirskoe sh. 31, Moscow 115409, Russia

E-mail: J.Knoll@gsi.de, F.Riek@gsi.de, Y.Ivanov@gsi.de, D.Voskresensky@gsi.de

**Abstract.** The effects of the propagation of particles which have a finite life-time and an according broad distribution in their mass spectrum are discussed in the context of a transport descriptions. In the first part some example cases of mesonic modes in nuclear matter at finite densities and temperatures are presented. These equilibrium calculations illustrate the dynamical range of spectral distributions to be adequately covered by non-equilibrium description of the dynamics of two nuclei colliding at high energies. The second part addresses the problem of transport descriptions which properly account for the damping width of the particles. A systematic and general gradient approximation is presented in the form of diagrammatic rules which permit to derive a self-consistent transport scheme from the Kadanoff–Baym equation. The scheme is conserving and thermodynamically consistent provided the self-energies are obtained within the  $\Phi$ -derivable two-particle irreducible (2PI) method of Baym. The merits, the limitations and partial cures of the limitations of this transport scheme are discussed in detail.

## 1. Scope of high energy nuclear collisions

Two atomic nuclei collide at high relative energies. During a time span of less than  $10^{-22}$  sec. a highly compressed and heated interaction zone is formed with matter densities  $\rho$  that exceed several times the nuclear saturation density  $\rho_0$  of 0.16 nucleon per cubic femto-meter ( $\text{fm}^3$ ) and temperatures  $T$  expressed in energy units beyond 100 MeV, cf. Fig. 1, below [1]. In daily life units this corresponds to  $\rho \geq 10^{15}$  g/cm<sup>3</sup> and  $T \geq 10^{12}$  K and thus to the highest matter densities and temperatures ever realized in laboratory experiments. Such matter conditions prevailed during the first few micro-seconds of the early universe, occur in super nova explosions and their remnants, the neutron stars at somewhat lower temperatures. This form of matter can only be investigated in the laboratory through nuclear collisions where one collects the reaction products emitted from the highly excited collision zone in sophisticated multi-particle detector arrangements. For a recent and comprehensive experimental overview see e.g. ref. [2]. In such experiments one distinguishes strongly interacting reaction products, such as hadrons, essentially nucleons and pions but also hadrons with other flavors like strangeness or charm from solely electro-magnetically interacting probes such as photons or lepton pairs (electrons-positrons or di-muons). While the former can only give a clear view back to the situation where the particles were essentially frozen out, i.e. the strong interactions cease, the latter are classified as penetrating probes. Once created these particles pass the collision zone essentially without further interaction. Such penetrating probes permit to look deeply into the interaction zone and are thus interesting as messengers from the compressed and heated matter.

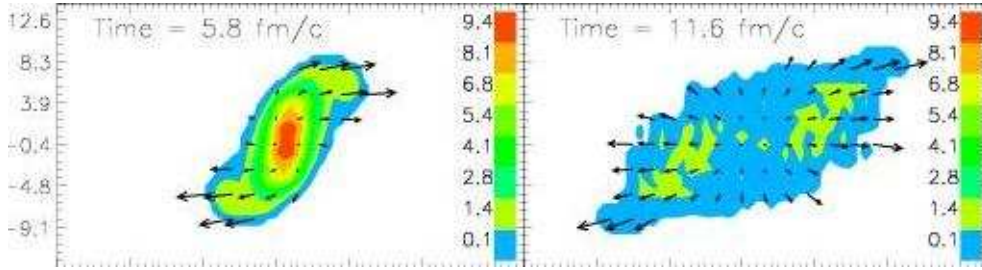


**Figure 1.** Collision of two gold nuclei at a bombarding energy per nucleon of 160 GeV. Contour plots of the densities in units of  $\rho_0$  at two time steps, resulting from a three-fluid hydrodynamical model [1].

The observation of di-leptons has received much attention over the last decade due to the observed enhancement of di-lepton pairs in the invariant mass region below the vector-meson masses [3,4] and the observed suppression of  $J/\Psi$ -mesons in central nuclear collisions compared to proton-proton collisions. With the recently completed HADES di-electron spectrometer GSI continues this research at lower bombarding energies. Considerable progress in mass resolution achieved by new pixel detectors for high energy muons has enabled new experimental results with unprecedented mass resolution [5,6].

The endeavor to investigate such nuclear collisions in experiments at GSI, CERN or at the RHIC-collider at the Brookhaven laboratory (BNL) strongly relies on adequate theoretical descriptions of the dynamics of such reactions. While a fully quantum mechanical or even field theoretical description is off reach, simplified approaches are considered that cover different dynamical ranges of applicability. With focus on the equation of state (EoS) of the interacting matter hydrodynamical models were investigated. Since a full instantaneous stopping to local equilibrium is not compatible with experimental observations, various kinds of multi-fluid models were considered to relax these constraints and to allow for a partial transparency between the different fluid components [1], cf. the example given in Fig. 1. Even further generalizations treated the abundances of the different constituents by non-equilibrium rate equations, while only the kinetic degrees of freedom and the pressure were considered to be in local equilibrium [7]. These approaches permit to address the issues of phase transitions e.g. between the hadronic and the quark-gluon plasma (QGP) phase and the underlying EoS.

At the microscopic level kinetic transport descriptions are in use. They describe the constituents of the matter as classical particles subjected to Newtonian forces and to stochastic collisions among the particles in terms of generalized Boltzmann equations which adopt mean fields and the statistics (Fermi-Dirac/ Bose-Einstein) of the particles. Thereby the collision term is essentially taken from binary-collision cross-sections. The relevant degrees of freedom may significantly change during the collision process. Due to the collisions among the incident nucleons the latter do not only change their momenta but rather also may get excited to baryon resonances, further more mesons and mesonic resonances can be created and at sufficiently high energy density the sub-hadronic degrees of freedom, the quarks and gluons, become liberated forming a QGP.

In such collisions one is confronted with the fact that the dynamics has to include particles like the Delta isobar or e.g. rho-meson resonances which have life-times of less than 2 fm/c already in the vacuum. The equivalently damping widths thus exceed values of 100 MeV. Also the collisional damping rates deduced from presently used transport codes are of the same order, whereas typical mean temperatures range between 50 to 150 MeV depending on beam energy. Thus, the damping widths of most of the constituents in the system can by no means be treated as a perturbation. As a consequence the mass spectrum of the particles in the dense matter is no longer characterized by a sharp delta-function but rather acquires a width due to collisions

and decays. One thus comes to a picture which unifies *resonances* that have already a width in vacuum due to decay modes with the "states" of particles in dense matter, that obtain a width due to collisions (collisional broadening).

The theoretical concepts for a proper many body description in terms of a real time non-equilibrium field theory were already devised by Schwinger [8], Kadanoff and Baym [9], and Keldysh [10] in the early sixties, extensions to relativistic plasmas followed by Bezzerrides and DuBois [11]. First investigations of the quantum effects on the Boltzmann collision term were given by Danielewicz [12], the principal conceptual problems on the level of quantum field theory were investigated by Landsmann [13], while applications which seriously include the finite width of the particles in transport descriptions were carried out only in recent times, e.g. refs. [12, 14–22]. For resonances, e.g. the Delta resonance, it was natural to consider broad mass distributions and ad hoc recipes have been invented to include this in transport simulation models. However, many of these recipes were not correct as they violated some basic principles like detailed balance (see discussion in ref. [14]), and the description of resonances in dense matter has to be improved [19–26]. A further conceptual problem in self-consistent resummation schemes concerns the proper renormalization of the (hidden) divergent loops in the scheme. In this question significant progress has recently been achieved [27–29].

In this contribution the consequences of the propagation of particles with short life-times are discussed. First we investigate at the example of nuclear matter at various temperatures a strongly interacting system in equilibrium. In particular the spectral properties of pionic modes in matter are explored. These pionic modes couple to vector mesons which through their electromagnetic decay into di-leptons (pairs of electron-positron or muons) are considered as special messengers of the dense matter phase. These example cases illustrate the properties of particles with broad damping width in dense matter environment. In the final part we discuss how particles with such broad mass-width can be described consistently within a transport theoretical picture.

We are going to argue that the Kadanoff–Baym equations in the first gradient approximation together with the  $\Phi$ -functional method of Baym [30] provide a proper frame for kinetic description of systems of particles with a broad mass-width. To this end, we discuss relevant problems concerning charge and energy–momentum conservation, thermodynamic consistency, memory effects in the collision term and the growth of entropy in specific cases [23].

## 2. Equilibrium properties of particles and resonances in dense nuclear matter

In nuclear physics quite a broad variety of concepts and methods are in use depending on the particular question raised. This is due to the non-perturbative nature of the interaction. For nuclear structure commonly non-relativistic concepts are used, nowadays with so-called realistic two-body interactions, supplemented with a three-body correction. There the essential question lies in the proper treatment of the short range and tensor correlations [31, 32] with unifying prospects in the low-energy limit of a derived effective interaction [33]. In such approaches the exchanged bosons which furnish the forces only implicitly enter the dynamics through the static two-body potentials.

For the here presented treatment with focus on high energy excitations the exchange bosons become dynamical. Therefore we employ an effective field theory picture with nucleons, and the Delta-isobar resonance as the main baryonic matter fields interacting via pion exchange for the long-range part of the interaction. This we supplement by a repulsive Migdal-type two-body interaction of zero range in order to provide proper saturation and other properties of nuclei. Interested in penetrating probes we extend the model to include the lightest vector mesons in the second part of this section. These vector mesons are discussed as important messengers about the dense nuclear environment produced in nuclear collisions, since they can be observed through their electromagnetic decay into electron-positron or muon pairs.



turns out to be sensitive to values of the Migdal parameters and the pion baryon form-factor  $F(q)$  employed in the model. Due to this form-factor, which is fitted to the  $\pi N$ -scattering data the  $\Delta$ -hole component appears only as a slight shoulder above the peak. For the resolution used in the calculations the well known zero sound component at zero  $T$  is invisible.

For higher temperatures all structures are broadened. It is clear that such structures can no longer be described by a quasi-particle picture. Rather one has to take due account of the fully dressed spectral distributions of the particles in the medium.

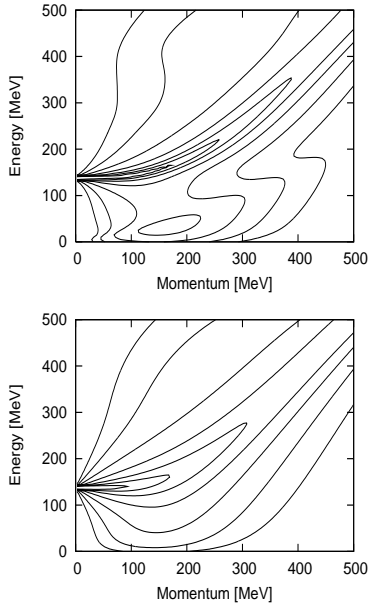


**Figure 2.** Contour plot of the logarithm of the pion spectral function  $A_\pi$  at  $T=0$  and 120 MeV (upper/lower panel) and  $\rho = \rho_0$ . The line spacing covers half a decade.

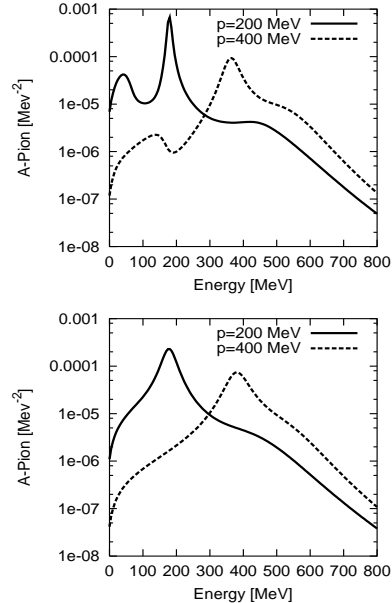


**Figure 3.** Pion spectral function  $A_\pi$  at  $T=0$  and 120 MeV (upper/lower panel) and  $\rho = \rho_0$  for two different momenta.

## 2.2. Vector-mesons coupled to the in-medium pion cloud

In view of the strong modifications of the pion spectral function through the dense nuclear medium it is interesting to study its influence on other modes that strongly couple to the pion, like the vector mesons, i.e. the  $\rho$ - and  $\omega$ -mesons. The vacuum widths of these resonances are generated through the decay into two pions in the case of the  $\rho$ -meson, respectively three pions for the  $\omega$ -meson. For the  $\omega$ -meson we choose the indirect decay via the  $\rho$ -meson (the so called Gell-Mann, Sharp and Wagner (GSW) process [40]) which is the dominant channel in vacuum. The coupling Lagrangian chosen in accordance with the low energy limit of QCD [41–43] gives rise to the following vector-meson polarization tensors (self-energies)

$$\Pi_\rho^{\mu\nu}(q) = \text{diagram 1} + \text{diagram 2} \quad \Pi_\omega^{\mu\nu}(q) = \text{diagram 3} \quad (2)$$

with four-momentum  $q = (q_0, \mathbf{q})$ . The two vector-meson coupling vertices are adjusted to the  $\pi\pi$ -scattering phase shifts together with the electromagnetic form-factor of the pion and to the vacuum decay width of the  $\omega$ -meson, respectively. For the numerical results we neglected the coupling of the  $\rho$ - $\omega$ -loop back to the pion as the vector mesons cause only a minor perturbation

to the  $\pi N \Delta$ -system. The correlation between  $\rho$ - and  $\omega$ -meson modes results from the  $\omega$ -meson self-energy (2) and the reverse process encoded in the coupling of the  $\rho$ -meson to the  $\omega$ - $\pi$ -loop which both are included self-consistently. Since the model omits higher lying degrees of freedom the in-medium changes of the real parts of the vector-meson self-energies are less precisely determined within the model space. Therefore we drop them during the self-consistent iterations, while restoring the normalization of the spectral functions at each step. A posteriori, with the parameters used we checked for the thus ignored real parts of the loops using a counter-term scheme which through vector dominance fixes the photon mass (i.e. at  $q^2 = 0$ ) to be zero with residue equal one in vacuum. It gave values of  $\text{Re}\Pi/(2q_0)$  which are by far less than the corresponding widths of the vector mesons and therefore negligible. Keeping this subtraction scheme also at finite  $T$ , i.e. ignoring contributions from hidden divergences [27] and tadpoles, which solely lead to an additional  $T$ -dependent mass shift, we still obtained insignificant changes in this quantity.

The resulting polarization tensors (2) have to be four-transversal because of current conservation. This is provided by a strategic projection method which uses two moments of the spacial part of the respective polarization tensors in the self-consistent loop approximation and constructs the respective four-transverse tensors. For details we refer to refs. [34, 44].

In the following we explicitly analyze the influence of the various components of the pion spectral function on the vector-mesons and thus on the di-lepton spectra. Formally we do this by splitting the spectral function of the vector-meson into the various components related to the different processes feeding into this vector-meson channel. Thus, decomposing the total damping width into partial widths  $\Gamma_{v,\text{tot}}(q) = \sum_i \Gamma_{v,i}(q)$ , the di-lepton yield can be brought into a Breit-Wigner like form with partial in- and out-widths

$$\begin{aligned} \frac{dR}{d^4q d^3x dt} &= \frac{3}{(2\pi)^4} f_T(q_0) \sum_v A_v(q) (-2\text{Im}\Pi_{v,e^+e^-}) \\ &= \frac{3}{(2\pi)^4} f_T(q_0) \sum_{v,i} \frac{4 q_0^2 \Gamma_{v,i} \Gamma_{v,e^+e^-}}{(q^2 - m_v^2)^2 + q_0^2 \Gamma_{v,\text{tot}}^2} \end{aligned} \quad (3)$$

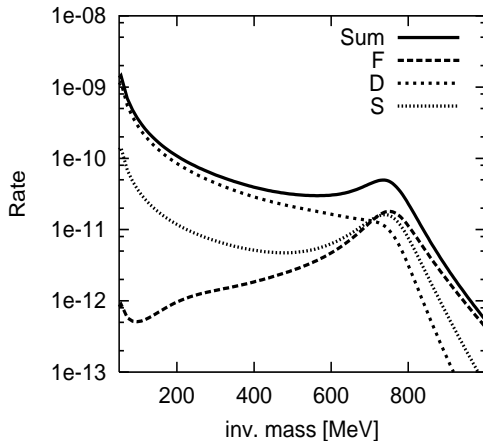


**Figure 4.**  $e^+e^-$ -rate from the decay of the  $\omega$ -meson at  $T=120$  MeV,  $\rho = \rho_0$  divided into different contributions:

- F:  $\pi\rho \rightarrow \omega$
- D:  $\rho \rightarrow \pi\omega$
- S:  $\rho N \rightarrow \omega N$ .

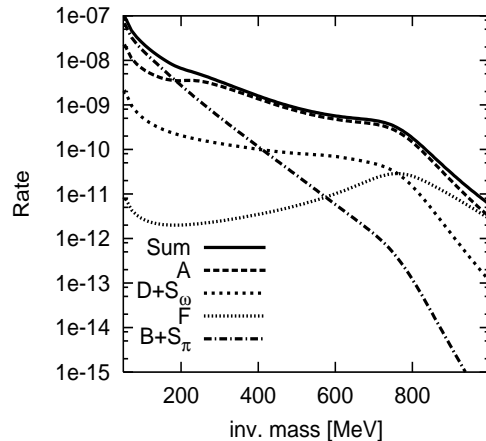


**Figure 5.**  $e^+e^-$ -rate from the decay of the  $\rho$ -meson at  $T=120$  MeV,  $\rho = \rho_0$  divided into different contributions:

- A:  $\pi\pi \rightarrow \rho$
- B:  $\pi \rightarrow \pi\rho$
- $S_\pi$ :  $\pi N \rightarrow \rho N$
- F:  $\pi\omega \rightarrow \rho$
- D:  $\omega \rightarrow \pi\rho$
- $S_\omega$ :  $\omega N \rightarrow \rho N$ .

(suppressing the tensor structure of spectral function and polarization tensor which leads to a degeneracy factor 3 for vector particles). Here  $m_v$  denotes the vector meson mass,  $f_T(q_0)$  is

the thermal Bose-Einstein distribution and  $\Gamma_{v,e^+e^-} = -\text{Im}\Pi_{v,e^+e^-}/(2q_0)$  is the di-lepton decay width of vector-meson  $v$ . In the vector dominance picture the vector mesons directly couple to a virtual photon which then decays into the respective lepton pairs, where for massless leptons  $\Gamma_{v,e^+e^-} \propto \alpha^2 m_v^4/(2q_0 q^2)$  with fine-structure constant  $\alpha$ .

We start the discussion of the effects on the  $\omega$ -meson. In the medium there are three major processes contributing to its damping width, illustrated by perturbative “time-flow” diagrams where the time is running from left to right and vertical lines denote virtual space-like propagators, which mediate two-body interactions:

$$(F) = \begin{array}{c} \rho \\ \text{wavy} \\ \text{---} \\ \text{---} \\ \pi \end{array} \begin{array}{c} \text{---} \\ \text{---} \\ \omega \end{array} \quad (D) = \rho \begin{array}{c} \text{---} \\ \text{---} \\ \text{---} \\ \pi \end{array} \begin{array}{c} \text{---} \\ \text{---} \\ \omega \end{array} \quad (S) = \begin{array}{c} \rho \\ \text{wavy} \\ \text{---} \\ \text{---} \\ \pi \end{array} \begin{array}{c} \text{---} \\ \text{---} \\ \omega \end{array} \quad (4)$$

The subsequent decay of the  $\omega$ -meson into the virtual time-like photon and its final decay into the lepton pair is not illustrated. In the self-consistent calculation with finite width spectral functions all these processes are included automatically by one self-energy diagram. For the first fusion-type process (F),  $\rho\pi \rightarrow \omega \rightarrow e^+e^-$ , the  $\omega$ -meson is formed by the fusion of a  $\rho$ -meson with a time-like in-medium pion. Its inverse exists already in vacuum and determines the vacuum decay width of the  $\omega$ -meson. The second process (D),  $\rho \rightarrow \pi\omega \rightarrow \pi e^+e^-$ , corresponds to a  $\rho$ -Dalitz-decay via an intermediate  $\omega$ -meson. In the self-consistent calculations, both above mentioned processes just differ in the sign of the pion energy in the  $\pi\rho$ -loop of the  $\omega$ -self-energy (2). The process (S) in (4) corresponds to the scattering  $\rho N \rightarrow \omega N$  mediated by a virtual, i.e. space-like pion exchange. In view of the pion modes at zero temperature (cf. Fig. 2) we isolate this space-like component by a cut on the far space-like region with pion loop momenta with  $|\mathbf{p}| > 2|p_0|$  in (2). At  $T = 120$  MeV this separation is less evident in view of the broad structure of the pion spectral function (Fig. 3). Thus the different components of the processes displayed in Fig. 4 somewhat depend on this cut. In addition to the fusion width (F), which constitutes just a temperature dependent modification of the vacuum width (e.g. accounted for by Schneider and Weise [45]) a genuine in-medium process, namely the scattering process (S), contributes with comparable strength at the nominal resonance position. The “Dalitz”-decay of the  $\rho$ -meson (D) dominates the low mass region.

In summary of this analysis: a major portion to the  $\omega$  spectrum results from processes (S) which are not accounted for in the simple on-shell treatment. These contributions, however, sensitively depend on the in-medium properties of the virtual pion cloud, which certainly needs further clarifying investigations before quantitative conclusions can be drawn.

The same type of processes as in (4) also occur for the  $\rho$ -meson just interchanging  $\rho$  with  $\omega$ , listed in the  $\rho$ -meson decomposition given in Fig. 5 as (F), (D) and ( $S_\omega$ ). However, these  $\omega$ -induced components are less important compared to the coupling to the two-pion channels given by

$$(A) = \begin{array}{c} \pi \\ \text{---} \\ \text{---} \\ \pi \end{array} \begin{array}{c} \text{---} \\ \text{---} \\ \rho \end{array} \quad (B) = \pi \begin{array}{c} \text{---} \\ \text{---} \\ \text{---} \\ \pi \end{array} \begin{array}{c} \text{---} \\ \text{---} \\ \rho \end{array} \quad (S_\pi) = \begin{array}{c} \pi \\ \text{---} \\ \text{---} \\ \pi \end{array} \begin{array}{c} \text{---} \\ \text{---} \\ \rho \end{array} \quad (5)$$

At invariant masses above 300 MeV, the  $\pi^+\pi^-$ -annihilation process (A) is clearly dominant. Processes (B) and ( $S_\pi$ ) are not present in any on-shell treatment of the pion as they solely arise from genuine off-shell components of the pion spectral function. In this respect (B) can be interpreted as a bremsstrahlung process radiated off a pion scattered in the medium,

while process (S) corresponds to inelastic  $\pi N \rightarrow \rho N$  scatterings mediated via virtual pion exchange. The latter two components, which emerge completely consistently within the model, only contribute to the very low-mass part of the invariant mass spectrum.

### 3. Conserving non-equilibrium dynamics of particles and resonances

The equilibrium results discussed above can immediately be implemented into a hydrodynamical scheme which relies on the assumption of local equilibrium. This concerns the EoS derived from the corresponding thermodynamic potential, as well as the spectral properties of the particles and resonances as the electromagnetic decay rates. As penetrating probes the latter can simply be integrated over the hydrodynamic space-time evolution, while strongly interacting probes require an appropriate freeze-out concept.

On the microscopic level the Kadanoff-Baym (KB) equations [9] provide the appropriate framework for a self-consistent dynamical treatment. However, only very recently first attempts to solve these equations for very simple scalar models were successfully undertaken [46, 47] in admittedly very simplified cases of simple scalar fields in spatially homogeneous systems. For the complex situations in nuclear dynamics substantial progress in computing power is required before meaningful calculation with the KB-equations can be performed. Therefore most applications are dealing with transport approaches where a Boltzmann-like transport equation is solved for the involved microscopic degrees of freedom. The numerical solution is mostly done by Monte Carlo simulation methods.

In this context one of the key issues was to generalize the concepts such that they can also properly deal with resonances or more generally with particles which have non-trivial i.e. non quasi-particle like spectral functions. The corresponding concepts were already laid out in the book of Kadanoff and Baym [9]. It involves a systematic gradient approximation of the Wigner transformed KB-equations, avoiding the step towards the quasi-particle approximation. Thereby the question of thermodynamic consistence and conservation laws is of vital importance. Is such a transport scheme thermodynamically consistent and are the conservation laws associated with the symmetries of the underlying theory fulfilled?

#### 3.1. $\Phi$ -derivable scheme and exact conservation laws

For self-consistent Dyson-resummation schemes and thus for the KB-equations the question of thermodynamic consistence and conservation laws was settled by Baym [30]. He showed that such schemes are conserving, if and only if all self-energies result from the functional variation of a functional, called  $\Phi$ , which is a functional of the self-consistent classical fields (one-point functions) and two-point propagators, see also [23]. The functional method initially introduced by Luttinger and Ward [48] and later reformulated in terms of path integrals became known as the CJT-formalism [49] in field theory according to the names of the authors. The  $\Phi$ -functional is given by two-particle irreducible (2PI) closed diagrams in accordance with the Lagrangian of the system expressed in terms of the self-consistent propagators and classical fields, while the vertices remain the bare ones.

With focus on the Kadanoff-Baym equations we discard the dynamics of the classical field for the further considerations and concentrate on the self-consistent dynamics of the propagators  $G(x, y)$ . In a  $\Phi$ -derivable scheme the self-energies are generated from the functional  $\Phi\{G, \lambda\}$  through the following functional variation<sup>1</sup>, cf. [23, 30]

$$-i\Sigma(x, y) = \mp \frac{\delta i\Phi\{G, \lambda\}}{\delta iG(y, x)} \times \begin{cases} 2 & \text{for real fields} \\ 1 & \text{for complex fields} \end{cases} \quad \text{where} \quad (6)$$

$$i\Phi\{G, \lambda\} = \left\langle \exp \left( i \int_C d^4x \lambda(x) \mathcal{L}^{\text{int}} \right) \right\rangle_{2PI} \quad (7)$$

(upper/lower signs refer to fermions/bosons). Here and in the following labels for the different species in the system and internal quantum numbers are suppressed. Taking all 2PI diagrams for  $\Phi$  provides the exact self-energy and two-point propagator of the theory. The space dependent coupling factor  $\lambda(x)$ , whose physical value is unity, is introduced to permit further variations, cf. Eq. (8) below.

The virtue of the  $\Phi$ -derivable scheme (6) is, that the diagrammatic series (7) of  $\Phi$  can be truncated at any level, without spoiling the conserving properties of the self-consistent scheme (6) for the Dyson-Schwinger or KB equations, see Eq. (14) below. The so constructed self-energies lead to a coupling between the different species in the system, which obey detailed balance generalizing the special recipes for broad resonances given in ref. [50]. It has been shown [30], see also [23], that such a self-consistent scheme is thermodynamically consistent and exactly conserving at the expectation value level of the conserved currents.

For local couplings the interaction energy density is given by a functional variation with respect to the interaction strength  $\lambda(x)$

$$\mathcal{E}^{\text{int}}(x) = \langle -\mathcal{L}^{\text{int}}(x) \rangle = - \left. \frac{\delta i\Phi}{\delta i\lambda(x)} \right|_{\lambda=1}. \quad (8)$$

The single-particle potential energy density is defined as

$$\mathcal{E}^{\text{pot}}(x) = \frac{1}{2} \int_{\mathcal{C}} d^4y [\Sigma(x, y)(\mp i)G(y, x) + (\mp i)G(x, y)\Sigma(y, x)] \quad (9)$$

here written for complex fields. Both,  $\mathcal{E}^{\text{int}}$  and  $\mathcal{E}^{\text{pot}}$ , enter the energy-momentum tensor (12).

The  $\Phi$ -derivable scheme (6) implies exact conservation laws for the Noether currents and the energy-momentum tensor [23] given by

$$\partial_\mu J^\mu(X) = 0, \quad \partial_\mu \Theta^{\mu\nu}(X) = 0 \quad \text{with} \quad (10)$$

$$J^\mu(X) = \sum_a \int \frac{d^4p}{(2\pi)^4} e v^\mu (\mp i) F(X, p), \quad (11)$$

$$\Theta^{\mu\nu}(X) = \int \frac{d^4p}{(2\pi)^4} v^\mu p^\nu (\mp i) F(X, p) + g^{\mu\nu} (\mathcal{E}^{\text{int}}(X) - \mathcal{E}^{\text{pot}}(X)). \quad (12)$$

Here

$$F(X, p) = \mp i G^{-+}(X, p) \quad (\text{alias} \quad \mp i G^{<}(X, p)) \quad (13)$$

denotes the distribution function in four-phase-space given by the four-Wigner transformation of the two-point propagators  $G^{-+}(x_1, x_2)$ , while  $e$  stands for any of the conserved charges and the kinematical factor  $v^\mu$  related to the four-velocity is define in (18) below.

### 3.2. Kadanoff-Baym equations and complete gradient approximation

We assume the reader to be familiar with the real-time formulation of non-equilibrium field theory on the so called closed time contour, ubiquitously used in this book. Since we will deal with general multi-point functions we use the more convenient “-+” contour-vertex notation of refs. [23, 51] rather than the more clumsy “< >” notation. In the following we follow the lines given in ref. [52]. The set of coupled KB equations on the time contour in “-+” notation<sup>2</sup> reads

$$(G_0^{-1}(-i\partial_1) - G_0^{-1}(-i\partial_2)) G^{-+}(1, 2) = \int_{\mathcal{C}} d3 (\Sigma(1^-, 3)G(3, 2^+) - G(1^-, 3)\Sigma(3, 2^+))$$

<sup>2</sup> The numbers 1, 2 and 3 provide short hand notation for space-time coordinates  $x_1, x_2$  and  $x_3$ , respectively, including internal quantum numbers. With superscript, like  $1^-$  and  $2^+$ , assigned to them, they denote contour coordinates with - and + specifying the placement on the time or anti-time ordered branch. For an arbitrary two-point function  $f$  its decompositions into the two branches of the contour are denoted as  $f^{kl}(1, 2) = f(1^k, 2^l)$  with  $k, l \in \{-, +\}$ . The match to the notation used, e.g., in refs. [9, 12] is given by  $f^{-+} = f^<; f^{+-} = f^>; f^{--} = f^c; f^{++} = f^a$ .

$$\equiv \mp C(1^-, 2^+) \quad (14)$$

and likewise for  $G^{+-}$ . Here

$$G_0^{-1}(p) = \begin{cases} p^2 - m^2 & \text{for relativistic bosons} \\ p_0 - \mathbf{p}^2/(2m) & \text{for non-rel. fermions or bosons.} \end{cases} \quad (15)$$

is the inverse free Green function in momentum representation. The upper/lower sign factors refer to fermions or bosons, respectively,  $G_0$  and  $G$  correspondingly denote the free and full Green functions. The driving term on the r.h.s. of Eq. (14), summarized by  $C$ , is a functional of the Green functions through the self-energies  $\Sigma$  contour folded with  $G$ . The real-time integration contour is denoted by  $\mathcal{C}$ .

As usual the step towards transport equations is provided by introducing the four-dimensional Wigner transforms for any two-point function  $f$  through

$$f(x, y) = \int \frac{d^4p}{(2\pi)^4} e^{-ip(x-y)} f\left(\frac{x+y}{2}, p\right). \quad (16)$$

or its inverse relation. The KB Eq. (14) then transforms to

$$v^\mu \partial_\mu F(X, p) = C^{-+}(X, p; \{G\}) \quad (17)$$

$$\text{with } F(X, p) = \mp i G^{-+}(X, p) \quad \text{and} \quad v^\mu = \frac{\partial}{\partial p_\mu} G_0^{-1}(p). \quad (18)$$

Here the r.h.s. of the KB equation is also expressed in terms of the Wigner transforms of all Green functions through (16). The final step is to expand the complicated r.h.s. of Eq. (17) to the first-order in space-time gradients, cf. Appendix A or [52] for more details. Then the *local* part of this r.h.s.,  $C_{(\text{loc})}^{-+}$ , defines the collision term. It entirely consists of *non-gradient terms*, where all the different mean positions  $(x_i + x_j)/2$  occurring in the various Wigner-Green functions are replaced by the externally given mean position  $X$  of the l.h.s., i.e.  $X = (x_1 + x_2)/2$  and the diagrams are to be evaluated as in momentum representation. The corrections for the displacement to the true coordinates of each Green function are then accounted for to first order in space-time gradients. Here we simply abbreviate the gradient terms by a  $\diamond$  operator defined in Appendix A acting on the *local* diagram expression

$$v^\mu \partial_\mu (\mp i) G^{-+}(X, p) = (1 + \frac{1}{2} \diamond) \left\{ C_{(\text{loc})}^{-+}(X, p) \right\}, \quad (19)$$

where

$$C_{(\text{loc})}^{-+}(X, p) = C^{-+}(X, p; \{G_{(\text{loc})}\}), \quad (20)$$

is a functional of the local Green functions  $G_{(\text{loc})} \equiv G(X, p)$ . Here and for all further considerations below, both, Green functions  $G(X, p)$  and self-energies  $\Sigma(X, p)$ , whenever quoted in their Wigner function form, are taken in *local* approximation, i.e. with  $X$  given by the external coordinate and  $\Sigma(X, p)$  void of any gradient correction terms. The gradient terms (see Appendix A) have the form that in the diagrams defining  $C_{(\text{loc})}$  pairs of Green functions are replaced by their space-time and momentum derivatives, respectively, just leading to equations linear in space-time gradients. Naturally the result of the  $\diamond$ -operation depends on the explicit form, i.e. diagrammatic structure, of the functional on which it operates. For the non-gradient term in Eq. (19), which defines the *local* collision term

$$C_{(\text{loc})}^{-+} = \mp \Sigma^{-k}(X, p) \sigma_{kl} G^{l+}(X, p) - (\mp) G^{-k}(X, p) \sigma_{kl} \Sigma^{l+}(X, p) \quad (21)$$

$$= \underbrace{\mp i \Sigma^{-+}(X, p) i G^{+-}(X, p)}_{\text{gain}} - \underbrace{(\mp) i G^{-+}(X, p) i \Sigma^{+-}(X, p)}_{\text{loss}}, \quad (22)$$

we give both, the diagram expression (21) and the normally quoted *value* expression (22). The latter simplifies due to a cancellation of terms which however survive for the order sensitive gradient operation. Here  $\sigma_{ik} = \sigma^{ik} = \text{diag}(1, -1)$  defines the “contour metric”, which accounts for the integration sense, and summation over the contour labels  $k, l \in \{-, +\}$  is implied.

The above quantum kinetic equation (19) has to be supplemented by a *local* Dyson equation for the retarded Green function [9]

$$(G^R(X, p))^{-1} = (G_0^R(p))^{-1} - \Sigma^R(X, p), \quad (23)$$

which together with Eq. (19) provides the simultaneous solution to  $G^{+-}$ . The full retarded Green function  $G^R$  depends on the retarded self-energy  $\Sigma^R = \Sigma^{--} - \Sigma^{-+} = \Sigma^{+-} - \Sigma^{++}$  again in *local* approximation.  $G_0^R$  is the free retarded Green function. Please note that equation (23) is just algebraic although it is obtained within the frame of the first-order gradient approximation.

In most presentations of the gradient approximation to the KB equations, Eq. (19) is rewritten such that the gradient terms are subdivided into different physical parts: on the one hand Poisson bracket terms describing drag- and back-flow effects which are pulled to the left side of the equation and in cases where the self-energy explicitly contains internal vertices an additional memory collision term  $C^{\text{mem}}$

$$\begin{aligned} v^\mu \partial_\mu F(X, p) + \{\text{Re}\Sigma^R, \pm iG^{+-}\} + \{\pm i\Sigma^{+-}, \text{Re}G^R\} &= C_{(\text{loc})}^{+-}(X, p) + C_{(\text{mem})}^{+-}(X, p). \quad (24) \\ \text{with } \mp C_{(\text{mem})}^{+-}(X, p) &= \Sigma_{(\text{mem})}^{-k}(X, p) \sigma_{kl} G^{l+}(X, p) - G^{-k}(X, p) \sigma_{kl} \Sigma_{(\text{mem})}^{l+}(X, p) \\ &= -\Sigma_{(\text{mem})}^{-+}(X, p) G^{+-}(X, p) + G^{-+}(X, p) \Sigma_{(\text{mem})}^{+-}(X, p), \quad (25) \\ &\text{value} \end{aligned}$$

where  $\Sigma_{(\text{mem})}(X, p) = \frac{i}{2} \diamond \{\Sigma(X, p)\}$  is only non-zero if internal vertices exist in  $\Sigma$ .

Depending on the questions raised either the here presented separation of the gradient terms or the compact formulation (19) is more advantageous. For the derivation of the conservation laws only a unified treatment of both, the Poisson brackets and memory collision terms, reveals the symmetry among these terms, which then displays the necessary cancellation of certain contributions such that the conservation laws emerge. Starting from Eq. (19) and using the diagrammatic gradient rules given in Appendix A one could indeed prove that a) the Noether currents (11) and b) the *local* approximation of the energy-momentum tensor (12) are exactly conserved. In particular for the latter derivation the diagram rules (A.2) to (A.7) where an essential help to isolate the proper counting of diagrams with terms proportional to the number of vertices contributing to  $\mathcal{E}_{\text{int}}$  in (12) and those proportional to the number of Green functions contributing to  $\mathcal{E}_{\text{pot}}$ .

### 3.3. Physical interpretation of terms

For the physical interpretation it is advantageous to introduce the spectral function  $A(X, p) = -2\text{Im}G^R(X, p)$  determined by the retarded equation (23), as well as the four-phase-space occupation functions  $f(X, p)$ , by means of  $F(X, p) = f(X, p)A(X, p)$ . In thermal equilibrium  $f(X, p)$  becomes a Fermi-Dirac or Bose-Einstein distribution in the particles energy  $p_0$ . The evolution of  $F$  is governed by transport Eq. (24) or equivalently by (19). Together with the retarded equation (23) this defines a generalized quantum transport scheme which is void of the usual quasi-particle assumption. The space-time evolution is completely determined by the initial values of the Green functions at time zero for each space point. Thus the evolution is “*Markovian*”, since the memory part of the collision term is kept up to first-order gradient terms only. Within its validity range this transport scheme is capable to describe slow space-time evolutions of particles with broad damping width, such as resonances, within a transport dynamics, now necessarily formulated in the four-dimensional phase-space.

Coming from the usual on-shell Boltzmann or Boltzmann-Uehling-Uhlenbeck collision term, each occurring three-momentum distribution function together with its momentum integration is simply to be replaced by its four-momentum analog, thus

$$f(X, \mathbf{p}) \frac{d^3 \mathbf{p}}{(2\pi)^3} \implies F(X, p) \frac{d^4 p}{(2\pi)^4} = f(X, p) A(X, p) \frac{d^4 p}{(2\pi)^4}. \quad (26)$$

Alongside the normally occurring two-body cross-sections have to be replaced by the corresponding  $T$ -matrix expressions providing the proper off-shell extensions. For genuine momentum dependent  $T$ -matrices the collision term has a finite virial due to the interactions at finite distances and therefore the collision term contributes to the conservation laws in a non-trivial fashion. Within field theory model applications with local couplings one simply has to evaluate the corresponding self-energies for the collision term. In this case the local collision term drops out of the conservation laws. With  $\Phi$ -derivable self-energies the collision term assures detailed balance.

More subtle are the first order gradient terms given by the two Poisson brackets and the memory collision term in Eq. (24). All three terms contribute to the conservation laws. Thereby the first Poisson bracket furnishes the so-called drag-flow. In the quasi-particle limit it accounts for the dressing of the particles by the dragged matter cloud as to form a quasi-particle with a non-trivial dispersion relation with a corresponding in-medium group velocity that can be expressed by an effective mass. This change in flow is just compensated by the second Poisson bracket through the polarization of the medium. The latter thus forms a back-flow component. Only the coherent play of both Poisson brackets restores the conserved Noether currents and thus recovers e.g. Galilei (Lorentz) invariance.

Since the first Poisson bracket involves space-time and momentum gradients directly acting on the distribution function  $F$  this term has an easy classical interpretation where the motion of the corresponding particle is subjected to a force which generally is momentum dependent. A generalization of this concept to the four-momentum picture is straight forward, since it just amounts to establish the corresponding characteristic curves of the homogeneous first-order differential equation. For the second Poisson bracket term on the other hand the derivatives of the distribution function appear only implicitly through the self-energy with the result that they affect momenta other than the momentum externally entering the transport equation. This has to be such, since the discussed term describes the reaction of the surrounding matter on the particle moving through the matter. However this term escapes an immediate description in terms of test particles, such that a simulation algorithm could not yet be established for the exact quantum kinetic equation (24).

Guided by equilibrium relations Botermanns and Malfliet [15] suggested a simplification of this second Poisson term, cf. [21, 22, 24]

$$\{-i\Sigma^{-+}, \text{Re}G^R\} \underset{\text{BM}}{\implies} \{f(X, p)\Gamma(X, p), \text{Re}G^R\} \quad \text{with} \quad \Gamma(X, p) = -2\text{Im}\Sigma^R, \quad (27)$$

formally valid up to second order gradient terms. Here the distribution function  $f(X, p)$  directly appears, while  $\Gamma$  is the damping width. The advantage of this substitution is that now the Poisson-bracket derivatives directly act on the distribution function  $f$  and the term amends a test-particle simulation [21, 22]. The price to be payed is that then the conservation laws are slightly modified, since instead of the spectral function  $A$  rather the entropy-spectral function  $A_s = \frac{1}{2}A\Gamma^2$ , as introduced in ref. [53], enters the conserved current expression

$$J_{\text{BM}}^\mu(X) = \int \frac{d^4 p}{(2\pi)^4} ev^\mu f(X, p) A_s(X, p)(X, p). \quad (28)$$

The BM-substitution accounts for part of the back-flow. In the quasi-particle limit both spectral functions converge to the same  $\delta$ -function at the quasi-particle energy [24, 53]. A further merit of the BM-substitution is that for certain collision terms an entropy current can be derived which fulfills an exact H-theorem, for details see ref. [24].

#### 4. Summary and prospects

The initially presented nuclear physics examples show that in the dense nuclear environment the particles acquire strongly broadened spectral functions. They reach damping widths which are of the same order as the systems temperature or even larger. Such spectral functions escape the conventional treatment within the quasi-particle limit.

For the application to nuclear-collisions dynamics problems the Kadanoff-Baym equations within a certain truncation level would certainly be the ultimate description level. However the required numerical afford presently limits such application to simple space-homogeneous systems and prevents realization in full three space dimension, time and four momentum space! Therefore we review the prospects of generalized transport equations derived in first-order gradient approximation from the KB-equations. Avoiding the quasi-particle limit the resulting set of dynamical equations consists of a generalized transport equation and a retarded equation for each type of particle in the system.

We conclude that the resulting equations posses remarkable properties if derived in a so called  $\Phi$ -derivable scheme. There the driving terms, the self-energies, are generated from a functional of closed diagram, the  $\Phi$ -functional, of the non-equilibrium Green functions that can be truncated at any level. Thereby the transport equation consists of a local collision term which obeys detailed balance and first order gradient terms. In their exact form the first order gradient terms guarantee exactly conserved Noether currents and a conserved energy-momentum tensor (the latter provided that local couplings are used). In thermal equilibrium they furnish a non-trivial equation of state in accordance with the truncation level of  $\Phi$ . The equations of motion further preserve the retarded properties of the real-time components of the contour Green functions. Thus, the dynamical equations provide a *generic* scheme for a proper treatment of the motion of particles and resonances with non-trivial, i.e. finite mass-width spectral functions. Certain gradient terms escape an immediate numerical simulation in terms of classical test particles. However first numerical applications [46] with the Botermanns-Malfliet substitution [15, 22, 24] look promising.

Initially we aimed at a proper transport description for broad resonances. However the presented schemes with dynamical spectral functions offers even more. Already at the lowest order self-energy level (genuine two-point function with no further internal vertices), which leads to a collision term and therefore to a finite damping width, the scheme provides the following advantages:

- the scheme includes higher order processes such as Bremsstrahlung which would be absent at the very same diagram level in the quasi-particle approximation;
- it leads to completely regular expressions at any order of the self-energy; in order to avoid double counting and the inclusion of redundant processes which are generated from lower order processes through the iteration of the equations of motion, higher order self-energy terms have just simply to be derived from a 2PI generating functional;
- therefore it avoids serious conceptual problems that arise in the use of the quasi-particle approximation for higher order processes (multi-particle scattering). The latter lead to mathematically ill defined expressions (squares of delta-functions or principle values) for the collision term which precisely arise whenever an intermediate propagator kinematically acquires on-shell conditions. The latter processes are precisely the reducible ones, as they can be generated through an iteration of lower order processes. Within the quasi-particle

picture there is no clear cut way to avoid such complications and mathematical pathologies. Only partial resummation schemes such as the Dyson resummation with finite damping width spectral functions can cure this problem.

The partial resummations implied by the self-consistent Dyson or KB scheme lead to violations of Ward-Takahashi identities for higher order correlation functions. In the context of vector mesons this affects the current conservation of the polarization tensor. As we briefly discussed, special projection strategies [34, 44] can be used to recover the four transversality. Also in cases of spontaneously broken symmetries the Nambu-Goldstone theorem is violated as the self-consistent Goldstone-boson masses are non zero. Recently the authors [54] suggested a correction term to the  $\Phi$ -functional which recovers massless Goldstone bosons in the broken phase.

In conclusion, the generalized transport equations together with the  $\Phi$ -derivable concept represent a generic dynamical scheme to deal with particles which attain broad spectral functions. In addition to the merits of this approach there are prospects that some of the deficiencies can be cured by adapted corrections without leaving this conceptual frame. E.g. with applications to Quantum Chromodynamics (QCD) in mind this gives hope that at a proper time also non-trivial self-energies can be treated for the case of gauge fields.

### Acknowledgments

We are grateful to G. Baym, J. Berges, P. Danielewicz, B. Friman, H. van Hees, C. Greiner, E.E. Kolomeitsev, M. Lutz and S. Leupold for fruitful discussions on various aspects of this research. Two of us (Y.B.I. and D.N.V.) highly appreciate the hospitality and support rendered to us at Gesellschaft für Schwerionenforschung. This work was supported in part by the Deutsche Forschungsgemeinschaft (DFG project 436 RUS 113/558/0-2) and the Russian Foundation for Basic Research (RFBR grant 03-02-04008).

### Appendix A. Diagram rules for the gradient approximation

Let  $M(1, 2)$  be any two-point function with complicated internal structure. We are looking for its Wigner function  $M(X, p)$  with  $X = \frac{1}{2}(x_1 + x_2)$  to first-order gradient approximation. The zero-order term is just given by evaluating  $M(1, 2)$  with the Wigner functions of *all* Green functions taken at the same space-time point  $X = (x_1 + x_2)/2$  and the momentum integrations being done as in the momentum representation of a homogeneous system. To access the gradient terms related to any Green function  $G(i, j)$  involved in  $M(1, 2)$ , its Wigner function  $G(\frac{1}{2}(x_i + x_j), p)$  is to be Taylor expanded with respect to the space-time reference point  $X = (x_1 + x_2)/2$ , i.e.

$$G\left(\frac{x_i + x_j}{2}, p\right) \approx G(X, p) + \frac{1}{2} \left[ (x_i^\mu - x_1^\mu) + (x_j^\mu - x_2^\mu) \right] \frac{\partial}{\partial X^\mu} G(X, p). \quad (\text{A.1})$$

Both,  $\partial_X G(X, p)$  and the accompanying factors  $(x_i - x_1)$  and  $(x_j - x_2)$ , can be taken as special two-point functions, to which special diagrams can be assigned

$$\overline{\overline{i \quad j}} = \frac{1}{2} (\partial_i + \partial_j) G(i, j) \longrightarrow \partial_X G(X, p), \quad (\text{A.2})$$

$$\overline{\overline{i \quad \leftarrow j}} = -i(x_i - x_j) \longrightarrow -(2\pi)^4 \frac{\partial}{\partial p} \delta(p) \quad (\text{A.3})$$

with the corresponding Wigner functions on the right hand side. Then the gradient terms of any complicated two-point function (given in different notations) can graphically be represented by the following two diagrams on the r.h.s.

$$\diamond \{M(1, 2)\} = \diamond \begin{array}{c} \square \\ \bullet \quad \bullet \\ 1 \quad 2 \end{array} \equiv \diamond \begin{array}{c} \square \\ \bullet \quad \bullet \\ 1 \quad 2 \end{array} = \begin{array}{c} \overset{3}{\curvearrowright} \quad \overset{4}{\curvearrowleft} \\ \square \\ \bullet \quad \bullet \\ 1 \quad 2 \end{array} + \begin{array}{c} \overset{3}{\curvearrowleft} \quad \overset{4}{\curvearrowright} \\ \square \\ \bullet \quad \bullet \\ 1 \quad 2 \end{array} \quad (\text{A.4})$$

Here the diamond operator  $\diamond$  formally defines the spatial gradient approximation of the two-point function  $M$  to its right with respect to the two external points (1, 2) displayed by full dots. The diagrammatic rules are then the following. For any  $G(3, 4)$  in  $M$ , take the spatial derivative  $\partial_X G(X, p)$  (double line) and construct the two diagrams, where external point 1 is linked to 3 by an oriented dashed line, and where point 2 is linked to 4, respectively. Interchange of these links provides the same result. Here  $M'$  is a four-point function generated by opening  $M(1, 2)$  with respect to any propagator  $G(3, 4)$ , i.e.

$$M'(1, 2; 3, 4) = \mp \frac{\delta M(1, 2)}{\delta iG(4, 3)}. \quad (\text{A.5})$$

The diagrams in Eq. (A.4) are to be evaluated in the local approximation, i.e. with all Wigner Green functions taken at the externally given space-time point  $X$ . The dashed line (A.3) adds a new loop to the diagram, which, if integrated, leads to momentum derivatives of the Green functions involved in that loop. Both, double and dashed lines have four-vector properties, and the rule implies four-scalar products between them. From (A.3) follows that

$$\begin{array}{c} \text{---} \leftarrow \text{---} \\ 1 \qquad 3 \end{array} = \begin{array}{c} \text{---} \leftarrow \text{---} \\ 1 \qquad 2 \end{array} + \begin{array}{c} \text{---} \leftarrow \text{---} \\ 2 \qquad 3 \end{array} \quad \text{and} \quad \begin{array}{c} \text{---} \\ \bullet \end{array} \text{---} \text{---} = 0. \quad (\text{A.6})$$

In momentum representation these rules correspond to the partial integration. They also imply  $\diamond\{M(1, 2)\} = 0$ , if  $M$  contains no internal vertices. The convolution of two two-point functions gives

$$\begin{aligned} \diamond\{C(X, p)\} &= \diamond \left\{ \begin{array}{c} \text{---} \bullet \text{---} \\ \text{---} \bullet \text{---} \end{array} \right\} \\ &= \begin{array}{c} \text{---} \bullet \text{---} \\ \text{---} \bullet \text{---} \end{array} + \begin{array}{c} \text{---} \bullet \text{---} \\ \text{---} \bullet \text{---} \end{array} + \begin{array}{c} \text{---} \bullet \text{---} \\ \text{---} \bullet \text{---} \end{array} + \begin{array}{c} \text{---} \bullet \text{---} \\ \text{---} \bullet \text{---} \end{array} \quad (\text{A.7}) \end{aligned}$$

$$= \{A(X, p), B(X, p)\} + A(X, p)\diamond\{B(X, p)\} + \diamond\{A(X, p)\}B(X, P), \quad (\text{A.8})$$

$$\text{where} \quad C(1, 2) = \int_C d^3A(1, 3)B(3, 2).$$

Besides the Poisson bracket expression  $\{A, B\}$  it leads to further gradients within each of the two functions. Applied to the r.h.s. of Eq. (19), this rule indeed provides the decomposition into Poisson bracket and memory terms of the quantum kinetic equation (24).

## References

- [1] Ivanov Yu B, Russkikh V N and Toneev V D, nucl-th/0503088
- [2] Andronic A and Braun-Munzinger P 2004 *Lect. Notes Phys.* **652** 35; hep-ph/0402291
- [3] Adamova D et al, CERES collaboration, 2005 *Nucl. Phys. A* **749** 160
- [4] Ramello L et al, NA50 collaboration, 2003 *Nucl. Phys. A* **715** 243
- [5] Borer K et al, NA60 collaboration, *Nucl. Phys. A* **749** 251
- [6] S. Damjanovic, in Quark Matter 2005, <http://qm2005.kfki.hu>, to be published in *Nucl. Phys. A*
- [7] Barz H-W, Friman B L, Knoll J and Schulz H 1988 *Nucl. Phys. A* **484** 661  
Barz H-W, Friman B L, Knoll J and Schulz H 1990 *Nucl. Phys. A* **519** 831
- [8] Schwinger J 1961 *J. Math. Phys.* **2** 407
- [9] Kadanoff L P and Baym G 1962 *Quantum Statistical Mechanics* (Benjamin)
- [10] Keldysh L P 1964 *ZhETF* **47** 1515 [ 1965 *Sov. Phys. JETP* **20** 1018]
- [11] Beizerides B and DuBois D F 1972 *Ann. Phys. (N.Y.)* **70** 10
- [12] Danielewicz P 1984 *Ann. Phys. (N.Y.)* **152** 239
- [13] Landsmann N P 1988 *Phys. Rev. Lett.* **60** 1990  
Landsmann N P 1988 *Ann. Phys.* **186** 141
- [14] Danielewicz P and Bertsch G 1991 *Nucl. Phys. A* **533** 712
- [15] Botermans W and Malfliet R 1990 *Phys. Rep.* **198** 115

- [16] Herrmann M, Friman B L and Nörenberg W 1993 *Nucl. Phys. A* **560** 411
- [17] Henning P A 1995 *Phys. Rep.* **253** 235  
Henning P A 1995 *Nucl. Phys. A* **582** 633
- [18] Henning P A and Quack E 1995 *Phys. Rev. Lett.* **75** 2811  
1996 *Phys. Rev. D* **54**, 3125
- [19] Weinhold W, Friman B L and Nörenberg W 1996 *Acta Phys. Pol.* **27** 3249  
Weinhold W, Friman B L and Nörenberg W 1998 *Phys. Lett. B* **433**, 236
- [20] Knoll J and Voskresensky D N 1996 *Ann. Phys.* **249** 532  
Knoll J and Voskresensky D N 1995 *Phys. Lett. B* **351**, 43
- [21] Leupold S 2001 *Nucl. Phys. A* **672** 475  
Leupold S 2001 *Nucl. Phys. A* **695** 377
- [22] Cassing W and Juchem S 2000 *Nucl. Phys. A* **665** 377  
Cassing W and Juchem S 2000 *Nucl. Phys. A* **677** 445
- [23] Ivanov Yu B, Knoll J and Voskresensky D N 1999 *Nucl. Phys. A* **657** 413
- [24] Ivanov Yu B, Knoll J and Voskresensky D N 2000 *Nucl. Phys. A* **672** 313
- [25] Ivanov Yu B, Knoll J, van Hees H and Voskresensky D N 2001 *Phys. Atom. Nucl.* **64** 652
- [26] Ivanov Yu B, Knoll J and Voskresensky D N 2003 *Phys. Atom. Nucl.* **66** 1902
- [27] van Hees H and Knoll J 2002 *Phys. Rev. D* **65** 025010  
van Hees H and Knoll J 2002 *D* **65** 105005  
van Hees H and Knoll J 2002 *D* **66** 025028
- [28] Blaizot J-P, Iancu E and Reinoso U 2003 *Phys. Lett. B* **568**160  
Blaizot J-P, Iancu E and Reinoso U 2004 *Nucl. Phys. A* **736** 149
- [29] Reinoso U 2005 hep-ph/0510119
- [30] Baym G 1962 *Phys. Rev.* **127** 1391
- [31] Feldmeier H and Schnack J 2000 *Rev. Mod. Phys.* **72** 655
- [32] Neff T and Feldmeier H 2003 *Nucl. Phys. A* **713** 311
- [33] Bogner S K, Kuo T T S and Schwenk A 2003 *Phys. Rep.* **386** 1  
Schwenk A, these proceedings
- [34] Riek F and Knoll J 2004 *Nucl. Phys. A* **740** 287
- [35] Korpa C L and Malfliet R 1995 *Phys. Rev. C* **52** 2756
- [36] Lutz M F M 2003 *Phys. Lett. B* **552** 159
- [37] Migdal A B 1978 *Rev. Mod. Phys.* **50** No. 1 Part 1,  
Migdal A B, Saperstein E E, Troitsy M A and Voskresensky D N 1990 *Phys. Rep.* **192** 179
- [38] Dimitriev V F and Suzuki T 1985 *Nucl. Phys. A* **438** 697
- [39] Urban M, Buballa M and Wambach J 2000 *Nucl. Phys. A* **673** 357  
Urban M, Buballa M, Rapp R and Wambach J 1998 *Nucl. Phys. A* **641** 433
- [40] Gell-Mann M, Sharp D and Wagner W G 1962 *Phys. Rev. Lett.* **8** 261
- [41] Schwinger J 1967 *Phys. Lett. B* **24** 473
- [42] Wess J and Zumino B 1971 *Phys. Lett. B* **37** 95
- [43] Witten E 1983 *Nucl. Phys. B* **223** 422
- [44] van Hees H and Knoll J 2001 *Nucl. Phys. A* **683** 369
- [45] Schneider R A and Weise W 2001 *Phys. Lett. B* **515** 89
- [46] Juchem S Cassing W and Greiner C 2004 *Nucl. Phys. A* **743** 92
- [47] Aarts G and Berges J 2001 *Phys. Rev. D* **64** 105010  
Berges J, these proceedings
- [48] Luttinger J M and Ward J C 1960 *Phys. Rev.* **118** 1417
- [49] Cornwall J M, Jackiw R and Tomboulis E 1974 *Phys. Rev. D* **10** 2428
- [50] Danielewicz P and Bertsch G *Nucl. Phys. A* 1991 **533** 712
- [51] Lifshiz E M and Pitaevskii L P 1981 "Physical Kinetics" *Pergamon press*
- [52] Knoll J, Ivanov Yu B and Voskresensky D 2001 *Ann. Phys. (NY)* **293** 126
- [53] Carneiro G M and Pethick C. J 1975 *Phys. Rev. B* **11** 1106
- [54] Ivanov Yu B, Riek F and Knoll J 2005 *Phys. Rev. D* **71** 105016  
Ivanov Yu B, Riek F, van Hees and Knoll J 2005 *Phys. Rev. D* **72** 036008